A Combined Experimental and Analytical Modeling Approach to Understanding Friction Stir Welding

Arthur C. Nunes, Jr.[1]
Michael B. Stewart[2]
Glynn P. Adams[2]
Peter Romine[3]

Abstract

In the Friction Stir Welding (FSW) process a rotating pin tool joins the sides of a seam by stirring them together. This solid state welding process avoids problems with melting and hot-shortness presented by some difficult-to weld high-performance light alloys. The details of the plastic flow during the process are not well understood and are currently a subject of research. Two candidate models of the FSW process, the Mixed Zone (MZ) and the Single Slip Surface (S^3) model are presented and their predictions compared to experimental data.

Introduction:

Friction Stir Welding (FSW) is a process developed at The Welding Institute (TWI) in England. The method uses large strain plastic deformation to join two pieces of material. The material is mechanically deformed using a rotating tool, which is forced along the weld seam. The mechanisms, which cause the bond, are believed to involve effects similar to those produced during forging and extrusion processes. Beyond this, little is actually known although many people working in the field are willing to speculate on the detailed mechanisms involved. Some measurements made using sacrificial thermocouples at the weld joint of aluminum alloys indicate that the maximum temperature during the weld process is on the order of 370C - well below the melting temperature of the material. However, at this temperature, the material properties are highly temperature dependent. The yield stress is approximately an order of magnitude less at this temperature than it is at room temperature

A schematic of the FSW process as applied to a butt joint is shown in Figure 1. The process will be described in reference to this type of weld. The main components required to conduct the friction stir weld include the pin tool, the anvil (backing bar) and the plates to be welded. The pin tool consists of a hardened steel tool with a large diameter shoulder and a smaller diameter threaded probe. The anvil is a flat, rigid steel plate. The aluminum plates, which are to be joined, are rigidly clamped to the anvil to prevent lateral movement and deflections relative to the anvil. This configuration can be obtained using a conventional milling machine with the anvil secured to the mill bed and the pin tool held by the spindle. The pin tool is rotated at a prescribed speed and tilted at a fixed lead angle. When the FSW process is initiated, the pin tool is not in contact with the plates. The pin tool is then plunged into the plates such that the trailing edge of the shoulder is slightly below the top surface of the plates. The dimensions of the pin tool are such that in this position, the probe of the pin tool is above the top surface of the anvil.

[1] NASA Marshall Space Flight Center, Huntsville, AL
[2] University of Arkansas, Fayetteville, AR
[3] Alabama A&M University, Huntsville, AL

Traversing the weld seam with the rotating tool completes the friction stir weld. The exact mechanisms that define the friction stir welding process are not completely understood. However, FSW is best described in conventional processing terms as a combination of extrusion and forging.

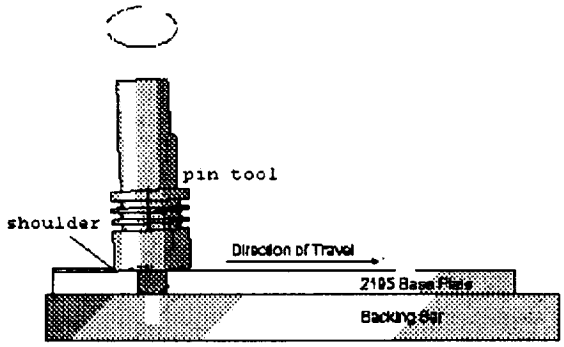

Figure 1 Schematic of friction stir welding process.

Figure 2 contains a picture of the weld cross section, which has been polished and etched. In this picture some interesting features of the weld are visible. At the top of the weld are extrusions caused by the rotation of the shoulder on the top of the weld. The shoulder entrains some material as it rotates, but the extent is not completely clear. It appears that the weld plug is roughly cone shaped with the top larger than the bottom although it is questionable to interpret these images in any detail. An interesting feature of this picture is the secondary swirl seen as a vortex like structure in the center of the image. This would actually be a long, two-dimensional roll aligned along the weld. Its importance, if any, is not clear.

There is little agreement among those working with friction stir welding, and less published, concerning the physical mechanisms important to the weld process. At the Friction Stir Welding Workshop held at Marshall Space Flight Center in February 1997 a number of conflicting perceptions of the FSW process were voiced, some formally and others informally.

In one perception the principal rotational slip takes place at the tool-workpiece interface. The workpiece metal, heated and softened by friction at the interface between tool and workpiece, flows back around the tool in a simple fluid stream like an extrusion and bonds behind the tool due to the high temperatures and pressures there. This perception does not seem consistent with the high degree of mixing and the central swirl observed in FSW beads and will not be discussed further.

Another perception has the principal rotational slip taking place not at the tool-workpiece interface, but expanded in a plastic zone rotating about the tool. The metal in the plastic zone flows in a vortex pattern matching the angular velocity of the tool at the tool-metal interface and dropping to zero at the edge of the plastic zone. The perception is analyzed here as the "Mixed Zone (MZ)" model. Incompatibility of mechanical and thermal equilibria in this model implied torque oscillations. Although oscillations were observed, none could be clearly attributed to this source.

A third perception has the principal rotational slip taking place at a contracted slip surface *outside* the tool-workpiece interface. The workpiece metal wipes onto the forward part of the slip surface and wipes off again behind the slip surface with the plug of metal surrounding the tool inside the slip remaining in place substantially unchanged once established. This perception is analyzed here as the "Single Slip Surface (S^1)" model.

Force measurements have provided considerable input to the understanding of FSW. With the measurements of forces in all directions and previous measurements of temperature, it is possible to argue more knowledgeably between conceptual models by using force (or moment) and energy balances. In this paper, conceptual models are proposed and evaluated based on force and energy balances

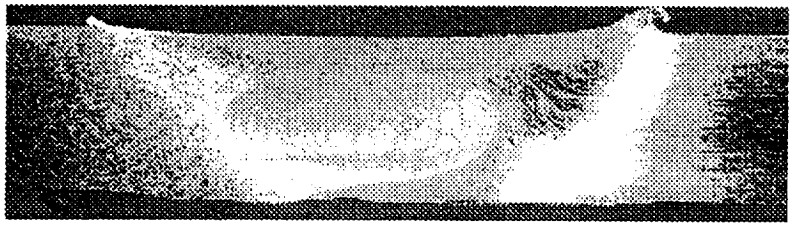

Figure 2 Photograph of FSW Cross Section

Measurements:

The mechanisms behind the friction stir welding process have been difficult to identify. At least part of the problem is due to the complexity of the process and the need to simplify and extract only the important features.

The welding process begins by creating a butt joint with the two plates, which are to be joined. The rotating tool is then forced between the two plates to a depth where the shoulder is slightly below the top surface of the material. This process forms a hole in the joint and, presumably, a region of deforming material. The tool is moved along the length of the joint and is withdrawn at the end of the weld. Another feature of the tool forces the material downward and the shoulder is assumed to add pressure to the deforming material and constrain it from flowing out of the plane of the plates. This configuration has evolved during the development of FSW and little or none of it has been rigorously proven.

Understanding of the mechanisms involved during the FSW process has been improved by the use of a rotating force dynamometer to measure the forces induced on the pin tool. The dynamometer serves as a tool holder, providing an interface between the spindle and the pin tool. This instrument provides the capability to measure the torque associated with rotating the tool (torque along the z-axis) and the axial load on the tool (thrust load along the z-axis). In addition a set of orthogonal rotating forces can be measured in the plane of the welded material. These forces can be resolved to transverse forces along the weld seam (x-axis) and forces perpendicular to the weld seam (y-axis).

With these measurements, all forces can be calculated for the moment balance and work into the weld material can be calculated for an energy balance. Figure 3 shows data for a typical 8-inch weld of ¼ inch aluminum plate.

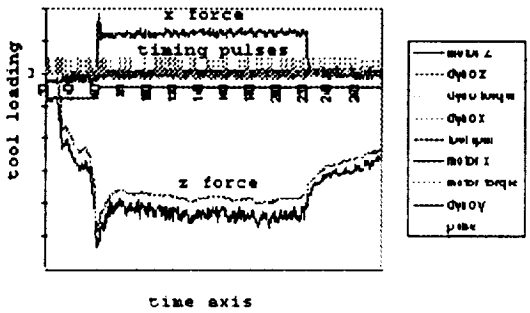

Figure 3 Dynamometer Measurements - FSW

The abscissa of the graph in Figure 3 is time in seconds. The two curves found in the bottom part of the graph represent the thrust force on the tool (z component). The smoother of the two is the dynamometer measurement and the rougher trace below the dynamometer curve is an estimate based on the current usage from the z-axis motor on the mill.

The final feature of interest in Figure 3 is the irregular spikes seen on the graph. These spikes represent pulses that are used for timing purposes. A pulse is sent to show the time when the dynamometer measured x force is pointing forward. In reality, the two measured forces in the plane of the weld material rotate with the tool and appear as two sinusoidal signals with a 90-degree phase shift. The timing signal indicates when one of these measurements, the "x" force, is oriented forward. Because of sampling variations, the pulses are captured irregularly and not every rotation of the tool. This is not important, as the phase shift between the maximum of the measured "x" force and the location of the pulse will be constant. Figure 4 shows the time axis enlarged. The spike appears as a triangular signal at a time of about 122 seconds. The peak of the triangle represents the location of the pulse and the finite width of the pulse signal is an artifact of the plotting algorithm - in fact the pulse signal is nonzero for a single measurement. The magnitude of the pulse is very large - on the order of 5000- and is reduced here for viewing purposes only. The location of the spike relative to the location of the maximum value of the "x" force shows that the force in the direction normal to the translation is small compared to the force in the direction parallel to the motion. That the normal force is not zero is due to the rotation of the tool causing an asymmetrical force. This will become clearer later when details of the models and comparisons are discussed.

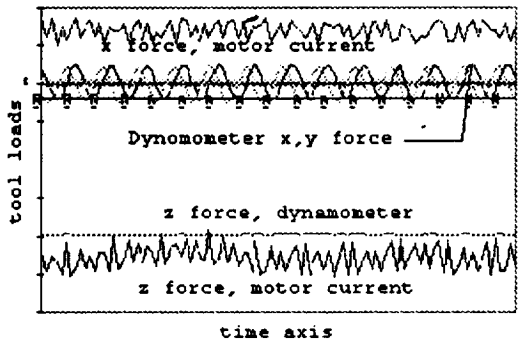

Figure 4. Time Axis Expanded

The other important measurement, which is too small in magnitude to be seen on Figures 3 and 4, is the tool torque. The measurement of torque is shown in Figure 5.

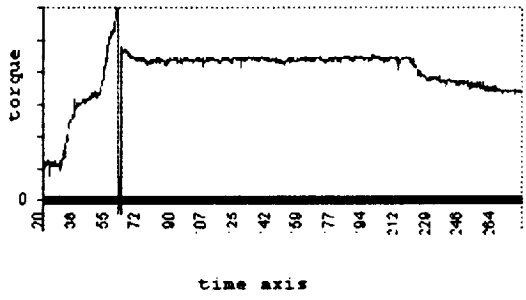

Figure 5 Dynamometer Torque Measurements vs. Time(s)

The measurements are small in magnitude but will be responsible for a majority of the effects in both the force and the energy balance as will be shown later. The period from 70s to 215s covers the actual weld event and is essentially steady state except for the possibility of a small amplitude oscillation.

Mixed Zone (MZ) Model:

Given these measurements, the difficult job of proposing and evaluating models is made much easier. An earlier model assumed that the weld material surrounding the pin tool was a continuously deforming 'pool' of material. An analysis of the required force balance was carried out earlier by one of the authors [1].

The first step is to assume a shear stress - temperature relationship i.e. $\tau = a(T-T_m)^n$ where τ is the flow stress, T is the local temperature, Tm is the melting temperature, and a is an empirical constant, and n is a positive integer chosen to fit the available data. Next, a force balance requires that the torque be in equilibrium. We consider an annular section of the weld plug bounded by two circles of radii r and r+dr. If the effects of the backing plate (the plate supporting the material from behind to react against the 5000 lbf of the tool into the material) on the torque is ignored; the two forces shown in the sketch must be equal. Thus, $d(2\pi r^2\tau)$ or, simplifying, $r^2\tau$ = constant. Using this relation we can write the forces at any position in terms of the forces at the pin surface (r=R).

$$\tau = \tau_R\left(\frac{R}{r}\right)^2$$

Finally, we can use the assumed relationship between temperature and flow stress to write,

$$a(T-T_m) = a(T_R-T_m)^n\left(\frac{R}{r}\right)^2$$

or,

$$T = T_m-(T_m-T_R)\left(\frac{R}{r}\right)^{\frac{2}{n}}$$

At the tool surface, R=r and $T = T_R$. In a typical non-dimensional form, this is written as,

$$\frac{(T-T_m)}{(T_R-T_m)} = \left(\frac{R}{r}\right)^{\frac{2}{n}}$$

FSW operates at temperatures always less than the melting temperature. As long as n is positive (a reasonable assumption) this temperature gradient conducts heat back towards the tool. There is no reasonable mechanism that allows the tool to be a heat sink of sufficient magnitude for this to occur.

This problem with the MZ model leads to the consideration of strain rate effects to produce reasonable predictions. The strain rate is commonly used in the literature to relate stress, strain, strain rate and temperature in constitutive relations for plastic deformation. Examples of these models are given by Miller [2], Besseling and van der Giessen [3], and Gilman [4]. These constitutive models form the basis for finite element (FE) predictions of plastic deformation such as the MatMod equations developed by Miller in 1987.

The effect of strain rate on the stress initially appears promising as a solution to the problem involving the equilibrium between torque and temperature effects. If we use the analogy with fluids, the strain rate and the resulting stress next to the tool surface would be a maximum and would diminish as we move away from the tool. The temperature field, in contrast, is hottest at the tool surface where the work input is greatest and diminishes with increasing radius. By combining the effects of stain rate and temperature, the motion in the flow field would adjust to maintain the required force balance. However, the temperature effect is much greater than the strain rate effect. Hence a large mixed zone cannot be maintained in equilibrium by a balance of the effects of stain rate and temperature. This is shown with the following simplified calculation.

Start by determining a functional relationship between temperature, strain and strain rate in the range of conditions found in FSW. Data is scarce but Miller exhibits some data. The FSW process has overall strain rates on the order of 300 to 400 per second (estimated using a plastic region extending from the pin surface to the outside of the shoulder at typical rotational speeds).

We are not interested in the overall strain rate but in the local values at different radial positions which will be considerably smaller than the overall value. We require that the total moment exerted at any radial position be constant. This balance requires $\tau_1 r_1^2 = \tau_2 r_2^2$. Miller's data was collected at two strain rates, .02 and 2.0 per second. For the purposes of making a simple estimate, a linear model of the

relationship between temperature and strain rate is assumed using Miller's data for a simple polycrystalline aluminum at saturation work hardening for each strain rate ([2] p. 170).

The calculations are made for an annular ring, bounded on the inside by r_1 and the outside by r_2 being continuously deformed at a temperature of 650K. The strain rate is assumed to be 2[1/s] at r_1 and a temperature of 600K and a strain rate of 0.02[1/s] at r_2. By balancing the moments at those two radii, a finite region which is deforming is predicted where $r_1 / r_2 = 1.02$. While this has the correct trend, the effect may be too small to account for the experimental observations. In Figure 6, calculated values of the relationship between r_1 / r_2 is plotted with values of the assumed temperature difference across the weld plug. This figure is generated using a very simplified analysis and should be used only to indicate rough estimates of the effects. The ratio $r_1 / r_{2\,max}$ be greater than 1. The trend is that a larger temperature difference requires the weld zone radius to decrease. The strain rates and temperature differences assumed in this calculation are for illustrative purposes only and are not necessarily representative of the process.

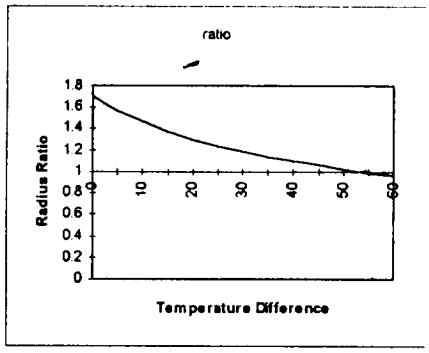

Figure 6: Outer to Inner Radius Ratio of Plastic Zone vs. Temperature Excess Required at Edge of Plastic Zone for Torque Equilibrium

To examine this issue of temperature effects compared to strain rate effect using a more realistic constitutive relationship, begin by assuming the slip process is thermally activated, so that

$$\dot{\varepsilon} = \dot{\varepsilon}_0 e^{\frac{E_0 - \tau\upsilon}{kT}}$$

E_0 is the activation energy

τ is the stress

υ is the "activation volume"

T is temperature, absolute

$\dot{\varepsilon}$ is the strain rate

$\dot{\varepsilon}_0$ is the maximum fully activated strain rate

Solving for τ,

$$\tau = \left(\frac{E_0}{\nu}\right) - \left(\frac{k}{\nu}\ln\dot{\varepsilon}_0\right)T + \left(\frac{k}{\nu}\right)T\ln\dot{\varepsilon}$$

Assuming that the temperature variations are small and using the data found in Miller, the stress may be approximated by

$$\tau = 97.7 + 3.02\ln\dot{\varepsilon}$$

Over a plastic zone extending from R to r the local strain rate is $-r d\omega/dr$ where ω is the local angular velocity. To balance the torque, the shear stresses at constant temperature become,

$$d\left[r^2\left(97.9+3.02\ln\left(-r\frac{d\omega}{dr}\right)\right)\right]=0$$

or,

$$r\frac{d^2\omega}{dr^2}+65.8\frac{d\omega}{dr}+2\frac{d\omega}{dr}\ln\left(-r\frac{d\ \omega}{dr}\right)=0$$

If the logarithmic term is ignored, the solution becomes,

$$\omega=\omega_0\frac{r_0^{64.6}}{R^{64.6}-r_0^{64.6}}\left[\left(\frac{R}{r}\right)^{64.6}-1\right]$$

Where r_0 is the inner radius of the deforming material and R is the outer radius. This function decreases rapidly from the value of the tool rotation at the inner radius resulting in a narrow region of significantly deforming materials. A simplification of this model is proposed in the next section and is used to predict tool forces and energy input.

Single Slip Surface (S^3) Model:

The relationship between the temperature difference and the extent of the weld zone leads to the development of an alternative model. In this model, the deforming region is restricted to a thin layer surrounding the pin tool. There is no reason to assume that the deforming layer will occur at the interface between the tool and the material. In fact, the geometry may consist of the pin tool, a mass of material surrounding the pin tool rotating at the same angular velocity, the deforming region modeled as a single slip surface, and stationary material lying outside of the weld region. For this geometry, heat is only generated in the deforming region. At steady state, the temperature of the material interior to the deforming region is nearly uniform and the exterior temperature decays with radius. This model will be referred to as the Single Slip Surface (S^3) model.

In its simplest form, the process looks like Figure 7 shown below. In this case, the weld plug rotates as a solid body at the same angular velocity as the tool. There is a large strain rate gradient over a small change in radius where all energy is input into the material. There is a discontinuity in the gradient of temperature at the slip region caused by the energy input. Without a significant heat removal mechanism, the temperature interior to the deforming region will be nearly uniform. The heat is conducted away from the weld plug with a negative temperature gradient outside the plug.

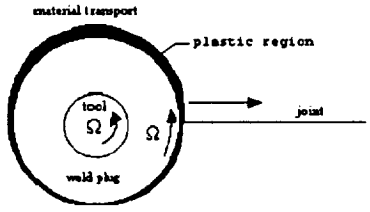

Figure 7. Sketch of the Single Slip Surface Model

Slip occurs only at the outer edge of the black layer seen in the sketch. In order for the tool to move through the weld material, the outer edge of the plug must entrain new material on the front of the weld plug, rotate it around to the rear and deposit it. Continuity or mass conservation requires that the layer of transported material is asymmetrical in shape about the transverse (or y) coordinate. The layer must have zero thickness at the bottom and maximum thickness at the top. There is little material convected into the weld plug so that the plug, once established, has very slow exchange with the weld material. Diffusion is the primary mechanism.

The Welding Forces:

The simplicity of this model makes it possible to calculate the required forces. The first estimate is the power dissipated at the slip surface. Both the temperature and geometry of the plug are assumed for this calculation. Using the geometry seen in Figure 2, the geometry is approximated as a tapered cylinder (see Figure 8). The required properties are the yield stress as a function of temperature. In the previous model (MZ), the yield stress was a function of both temperature and strain rate. The assumed mechanisms were creep and diffusion. In this model the single slip is assumed strain rate independent. The uniform temperature weld plug is assumed to be at 370C which is approximately the measured value. At this temperature the yield stress for aluminum alloy 2219 is 26MPa.

The required force will be, $F_x=\tau*$(area of the slip surface) or

$$F_x = \int \tau dA = \int_0^{z\,max} \tau 2\pi r(z)\sqrt{1+\left(\frac{dr}{dz}\right)^2}\,dz$$

And the resulting torque, which will be compared to the dynamometer measurements, is

$$T = 2\pi\tau \int_0^{z\,max} r^2(z)\sqrt{1+\left(\frac{dr}{dz}\right)^2}\,dz$$

The resulting estimate of power input, which is used for the prediction of the temperature field, is

$$\tilde{P} = 2\pi\tau\omega \int_0^{z\,max} r^2(z)\sqrt{1+\left(\frac{dr}{dz}\right)^2}\,dz$$

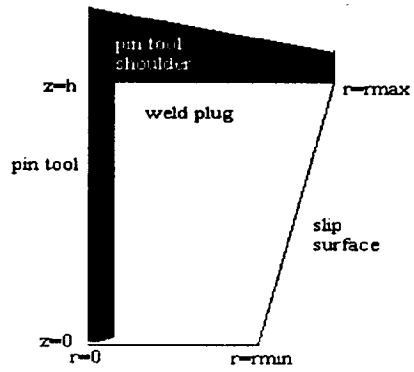

Figure 8. Hypothetical Geometry of Slip Surface in Relation to Pin Tool and Shoulder

The calculations are made by assuming a linear shape for the slip plane, fitting it to the observed shape shown in Figure 2, and using the experimental values of τ, ω, and the geometry of the tool and sample that was welded. The effect of the tool shoulder is to extend the radius of the weld plug at the top of the weldment. The bottom of the pin tool does not extend completely through the material. For the purposes of this estimate, the weld plug is assumed to extend completely through the material and slide over the anvil with little dissipation. The weld plug is modeled as a tapered cylinder with all dissipation occurring at the outer radius of the plug. The result of this calculation is P_{dis}.

The division of the power input between the rotational motion, the motion of the material into the weld, and the translation of the tool along the weld can be estimated. The moment is, approximately,

$$M \cong 2\pi hr^2\tau + \int_0^R 2\pi\xi^2\tau d\xi = 2\pi hr^2\tau\left(1+\frac{R^3}{3hr^2}\right)$$

The second term approximates the effect of the pin bottom and shoulder. r is the pin tool radius, R is the outer radius of the shoulder, τ is the shear stress between the weldment material and the tool, and h is the

material thickness. For the purposes of estimating the magnitude of each component, assume that h=2r and R=1.5r. In this case, $R^3/3hr^2=9/16$. With this geometry, the effect of the shoulder multiplies the torque by a factor of 1.56.

The translational force can be estimated using the model of a plastic indenter. This is, roughly,

$$F_x \cong 24hr\tau + \pi R^2\tau = 24hr\tau\left(1+\frac{\pi R^2}{24hr}\right)$$

Using the same dimensional estimates as before, $\pi R^2/24hr=3\pi/64$, the shoulder multiplies the translation force by 1.15.

$$\frac{F_x V_x}{M\omega} = \left(\frac{1.15}{1.56}\right)\frac{12V_x}{\pi r\omega}$$

At the feed rate, rotational speed, and material thickness used in the experiments, the translational power is approximately 11% of the rotational power.

Similarly, the forces into the weldment are estimated by

$$F_z \cong 2\pi hr\tau$$

If the thread pitch is p,

$$V_z \cong \omega p$$

so that

$$\frac{F_z V_z}{M\omega} = \left(\frac{1}{1.56}\right)\frac{p}{r}$$

Power F_zV_z is actually supplied by an increment of rotational power $\Delta M\omega = F_zV_z$. When the tool moves parallel to the workpiece as the force in the pin threads transforms F_z to an effective torque ΔM. If p =0.05 inches and r=0.25 inches, then the power to push metal down at the pin (so as to operate a secondary down and up circulation in the vicinity of the pin), the secondary circulation power is estimated at 0.13 times the pin rotational power.

Note that the z direction force obtained from the dynamometer measurements is much larger than F_z because the force measured by the dynamometer is not just the force doing work, but a stationary pressure force on the shoulder and pin bottom. From the analysis only a small part of the measured force actually does work.

If the pin tool is tilted through a lead angle θ such that it leaves a wake of depressed metal behind it, there is also what might be called an "ironing force" F_θ. Let the shoulder radius be R. Then the torque $M\theta$ rotating the metal back under the shoulder can be very roughly estimated by assuming a hemispherical mass of metal is rotated under the shoulder subject to surface shear τ:

$$M_\theta = 2\int_{y=0}^{y=R}\sqrt{R^2-y^2}\left(\pi\sqrt{R^2-y^2}\right)\left(\tau\frac{Rdy}{\sqrt{R^2-y^2}}\right) = 2\pi R^3\tau\int_{\frac{y}{R}=0}^{\frac{y}{R}=1}\sqrt{1-\left(\frac{y}{R}\right)^2}\,d\frac{y}{R} = \pi^2R^3\tau$$

Given weld speed V_x, the "ironing" power $P\theta$ is:

$$P_\theta = \pi^2R^3\tau\theta\frac{V_x}{2R}$$

The ironing power is supplied by an increment of the translational force

$$\Delta F_x = \frac{\pi^2R^2\tau\theta}{2}$$

The ratio of the ironing power to the rotational power is

$$\frac{P_\theta}{M\omega} = \frac{3\pi}{4}\left(\frac{\frac{R^2}{3hr^2}}{1+\frac{R^3}{3hr^2}}\right)\frac{\theta V_x}{R\omega} = 0.848\frac{\theta V_x}{R\omega} = .00236\frac{\theta[\text{degrees}]V_x[\text{inches/min}]}{R[\text{inches}]\omega[RPM]}$$

Given a lead angle of 2.5 degrees, a weld speed of 5 inches/minute, a shoulder radius of 0.5 inches and an RPM of 500:

$$\frac{P_\theta}{M\omega} = 0.01\%(negligible)$$

A slipping force F_s accompanies the tilting force. If a small slip velocity – V_x (in the travel direction) is superimposed upon the relative rotational velocity $r\omega(-\sin\theta\ U_x + \cos\theta\ U_y)$, then the shear force τda of element $da=rd\theta dr$ is presumed to act in the direction of relative slip velocity $(-r\omega\sin\theta - V_x)$ (the travel direction) + $(r\omega\cos\theta)$ (perpendicular to the travel direction). The projection in the direction of slip is

$$dF_s = -\tau r d\theta dr\left(\frac{r\omega\sin\theta + V_x}{\sqrt{(r\omega\sin\theta + V_x) + (r\omega\cos\theta)^2}}\right) = -\tau r d\theta dr\sin\theta\left(1 - 2\sin\theta\frac{V_x}{r\omega}\right)$$

assuming that $V_s << r\omega$. The integrated slip force is:

$$F_s = \int_{\theta=0}^{\theta=2\pi}\int_{r=0}^{r=R}\tau\left(-\sin\theta + 2\sin^2\theta\frac{V_x}{r\omega}\right)r dr d\theta = \frac{2\pi r V_x}{\omega}$$

The ratio of slip power to rotational power is:

$$\frac{F_s V_x}{M\omega} = 3\left(\frac{\frac{R^2}{3hr^2}}{1+\frac{R^3}{3hr^2}}\right)\left(\frac{V_x}{R\omega}\right)^2 = 0.0274\left(\frac{V_x[\text{inches/min}]}{R[\text{inches}]\omega[RPM]}\right)^2 = 0.001\%(negligible)$$

If the slip actually takes place over a surface r(z), where r is the distance from the tool centerline at depth z below the shoulder, in accordance with the S^3 model, then the estimates made above are upper bounds and the moment is actually

$$M = \int_{r=r_{min}}^{r=r_s} 2\pi r^2\sqrt{1+\left(\frac{dr}{dz}\right)^{-2}}\tau dr$$

Where r_{min} is the weld plug radius at the bottom of the weldment and r_s is the shoulder radius. In Figure 8 a hypothetical but reasonable shape of the slip surface is shown. The slip surface extends from under the tool to a radius r and then runs in a straight line a distance h to the shoulder of the tool at a radius R. For this shape the moment can be written as

$$M = \int_{r=0}^{r=r} 2\pi\xi^2\tau d\xi + \int_{r=r}^{r=R} 2\pi\xi^2\sqrt{1+\left(-\frac{R-r}{h}\right)^{-2}}\tau d\xi = \frac{\pi r^3}{3}\left[1+\left(\frac{R^3}{r^3}-1\right)\sqrt{1+\frac{1}{\left(\frac{R}{h}-\frac{r}{h}\right)^2}}\right]\tau$$

Given the proportions above, $M=2\pi hr^3\tau$. This is lower than the proportions used above, which are 1.56 times the value.

The Shape of the Slip Surface:

Out of all conceivable slip configurations, slip can first take place for the configuration offering least resistance. If this mode begins to operate, alternative modes requiring higher torque can never be attained. This presents a means for computing the shape of the slip surface in the context to the S^3 model by minimizing the moment M or, equivalently, the input power $M\omega$. This is a problem in the calculus of variations.

$$\delta \int_{r=r_{min}}^{r=r_s} 2\pi r^2 \sqrt{1+\left(\frac{dr}{dz}\right)^{-2}}\,\tau dr = 0$$

The problem is not as straightforward as it appears because the temperature rise generated by the plastic deformation alters the flow stress of the metal. Further, there is a question as to boundary conditions. The deforming surface will likely have one endpoint at the outside of the tool shoulder radius but the other endpoint may be either at the centerline under the tool or at a radius greater than the tool radius.

A solution was approximated using a very simple search algorithm with the following steps:

1) An initial shape is assumed
2) This shape is defined by a sequence of points with unique values of z and r
3) A sweep is initiated through the points where the radius of each point is adjusted both larger and smaller, the power required for the initial radius, the larger radius, and the smaller radius of the intervals on both sides of the point are calculated.
4) The radius is adjusted to the value corresponding to the minimum power value of the three values calculated
5) Steps 3 and 4 are repeated until the shape stops changing
6) End

The torque integral to be minimized expressed in finite element form is:

$$M = 2\pi r_i^2 \tau \sqrt{\left(r_{i+1} - r_i\right)^2 + \left(z_{i+1} - z_i\right)^2}$$

The search algorithm converged on a local minimum that may or may not be a global minimum or the actual physical shape of the surface. The minimum may be considered an upper bound, however, or would be if the shear stress approximation were good.

Calculations were made with a variety of initial conditions, number of points defining the surface, and allowable changes in the points. Some care was necessary in choosing the allowable change - too large and no change would be made, too small and convergence was slow. The calculated shape was insensitive to the number of points. Calculations were made with 10, 20, and 40 points and no visual change could be detected. Changes in initial conditions resulted in the same final shapes. Two cases are shown in Figures 9 and 10. Two contraints were used, the first being that the first point remains at the edge of the shoulder and the second was that none of the points could be inside the pin tool radius. All dimensions are in millimeters. The predicted shape is qualitatively similar to Figure 2. The second case modeled the bottom of the pin tool differently. In practice, the pin tool does not extend to the bottom of the material. Here, the radius of the bottom point was set at zero and the next two points were allowed to assume any radius. The other constraints were as before. Figure 2 shows a slight bulge at the bottom of the weld plug, which is not seen in either of this calculation, Figures 9 and 10. Given that this bulge is not part of the minimization requirement, it is likely that it comes from the downward movement of material caused by the rotation of the pin tool.

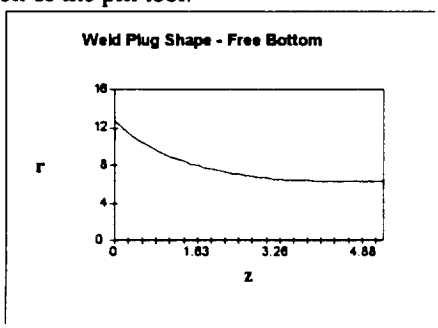

Figure 9. Computed Weld Plug Shape

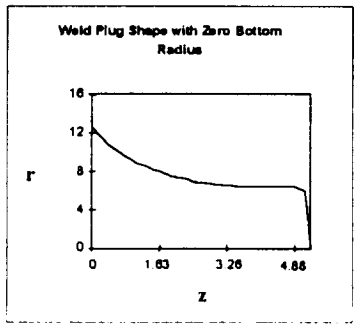

Figure 10. Computed Weld Plug Shape

This shape is close to the observed shape in Figure 2 and provides some support for this nonrigorous procedure. This example is intended to illustrate the method. A rigorous calculation requires the

simultaneous solution of the force equations on the slip surfaces, the simultaneous solution of the energy equations, and that both sets of equations are in equilibrium. Details of the shape could only be predicted by subdividing the domain and requiring internal energy and force equilibrium and external equilibrium with surrounding elements. The total work input was calculated using the assumed shape of the weld plug and the shear stress associated with the maximum temperature and this agrees with the experimental estimates of work input to within 10%.

The Temperature Field:

Temperature measurements taken during the FSW process show a maximum temperature below the melting temperature but above the recrystalization temperature. Measurements were made using a sacrificial thermocouple that limits measurements to the undeformed portion of the weld material. For the MZ model, this limitation is important because heat generation through friction is volumetrically distributed through the weld plug. For the S^3 model the limitation is unimportant because the heat generation is concentrated at the single slip plane and the weld plug is a uniform temperature with heat removal only by conduction outside the slip plane.

The energy E of the zone of plastic deformation that follows the tool remains constant under steady translation of the tool:

$$\frac{\partial E}{\partial t} = 0 \equiv \iiint \tau_{ij} \frac{\partial \gamma_{ij}}{\partial t} dv + \iint k \frac{\partial T}{\partial x_i} dA_i + \iint \rho e V_i dA_i$$

Where τ_{ij} = flow stress
γ_{ij} = plastic strain
dv = volume element
k = thermal conductivity
T = temperature
dA_i = area element (directed outward)
ρ = mass density of the weld material
e = specific energy of the weld material (both internal energy and plastic energy)
V_i = velocity field in weld material with respect to pin (includes negative pin velocity plus rotational field induced by pin rotation)

The first integral represents plastic work; the second integral, heat conduction losses, and the third, convection losses as the plastic zone picks up metal at initial temperatures and degrees of cold work and releases metal in different condition.

The plastic work integral can be equated approximately to the work input of the torque M and the translation force F.

$$\iiint \tau_{ij} \frac{\partial \gamma_{ij}}{\partial t} dv = M\omega + F_x V_x + F_z V_z$$

where M = torque
ω = angular velocity of the pin
F_x = translation force
V_x = translational velocity of pin
F_z = downward force at pin
V_z = downward velocity of flow at the pin

According to the computational estimates made previously, both F_xV_x and F_zV_z are substantially smaller than $M\omega$. The dynamometer measurements of the x component agree with this estimate. The z component dynamometer measurements indicate a high measured force, but much of the force is static and does not contribute to the energy input.

For a differential volume element in the vicinity of the pin tool

$$\frac{\partial e}{\partial t} = 0 \equiv \sigma_{ij}\frac{\partial \gamma_{ij}}{\partial t} + \frac{\partial}{\partial x_i}\left(k\frac{\partial T}{\partial x_i}\right) - \rho V_i \frac{\partial e}{\partial x_i}$$

Note that V_i in the convection term is the velocity field relative to the pin tool. Only outside the deformation field can it be equated to the translational velocity of the pin tool. Inside the plastic flow field energy is convected by the plastic flow as well as by the relative movement of the workpiece past the tool. The term ρV_i is moved outside the derivative on the basis that mass is conserved in the workpiece. The energy density of the workpiece metal changes with both temperature and the extent of deformation.

Outside the zone of plastic flow, the plastic work term vanishes, the energy may be written E=CT, where C is the specific heat of the metal, and k, unaffected by plastic deformation, may be considered constant. If the flow around the pin tool is approximately planar, i.e. if flow up and down the tool can be neglected, for a differential volume element moving with the pin tool:

An estimate of the maximum temperature can be made and compared to the measured value. We start with

$$\frac{\partial^2 T}{\partial x^2} + \frac{\partial^2 T}{\partial y^2} - \frac{V}{\alpha}\frac{\partial T}{\partial x} = 0$$

A simple line source of power P per unit depth located at the coordinate origin (x=0, y=0) and moving on a plate of fixed depth with insulated surfaces, in the x-direction with velocity V has the steady state solution [6]:

$$T(x,y) = \frac{\frac{P}{w}}{2\pi k}\exp\left(\frac{Vx}{2\alpha}\right)K_0\left(\frac{V\left[x^2+y^2\right]^{\frac{1}{2}}}{2\alpha}\right)$$

Where K_o is the modified Bessel functions of the second kind of order zero and P is is the energy input into the workpiece from the translation, rotation, and downward forces.

A friction stir weld can be represented roughly by a row of line sources over the segment $-b<x<+b$. If the total power per unit depth is P/w then at x' the source strength is $(P/2wb)dx'$.

$$T(x,y) = \frac{\frac{P}{w}}{2\pi k}\int_{-b}^{+b}\exp\left(\frac{Vx}{2\alpha}\right)K_0\left(\frac{V\left[(x-x')^2+y^2\right]^{\frac{1}{2}}}{2\alpha}\right)dx'$$

The integral is numerically integrated using a simple trapezoidal rule after non-dimensionalizing and substituting polynomial approximations [7] for the Bessel functions. The order of the numerical integration procedure was unimportant because the function is well behaved, the accuracy requirements are modest as this is a rough estimate, and a sensitivity study on the number of subdivisions showed that it converged rapidly.

Analytical prediction of the energy input into the weld material indicates that most comes from the angular motion. The power input to the weld material is also estimated from the dynamometer measurements. The work input from the measured rotation, translation, and downward force is used to estimate P/w. The input from the angular rotation supplied approximately 50% of power required to reproduce the maximum temperature at the deforming region with the thermal conductivity initially selected. The translational force, in agreement with the analytical calculations, supplied very little power compared to input from angular rotation. This is consistent with dynamometer measurements and also with a remark from J. McClure [8] on how easy it is for an individual to move the friction stir pin tool along the weld seam by manually turning the feed spindle on a milling machine. If the feed power were comparable to the pin rotational power, this would not be feasible.

The only input of work by the pin tool into the workpiece is through torque or translational forces, and these are known. (Downflow of the workpiece on the pin tool threads is accounted for by the additional

rotational torque included in the measurements.) So why does the temperature field appear to require twice as much power than the known power input? Note that the temperature field is sensitive to thermal conductivity k as well as to power P. Neglecting velocity effects, the temperature is proportional to the P/k. If k is halved, P/k is doubled. Errors in k amounting to a factor of x2 would not be impossible. If the thermal conductivity is sensitive to the defect structure, i.e. dislocations and anything else that may scatter phonons, of the alloy. Annealing near the weld increases local thermal conductivity. (Annealing 2219 aluminum from the T37 condition raises the thermal conductivity by about 46% [9], for example.) High strain rates may inject unstable dislocation structures in the plastic region that absorb energy and then release it at a later time so as to transfer heat by a kind of "phase transformation" mechanism. Thus the apparently low power is interpreted as caused by use of too high a thermal conductivity in the analysis.

The computed temperature profile had a maximum temperature that agreed well with measurements when P/k was corrected. The form of the temperature profile is shown in Figure 11.

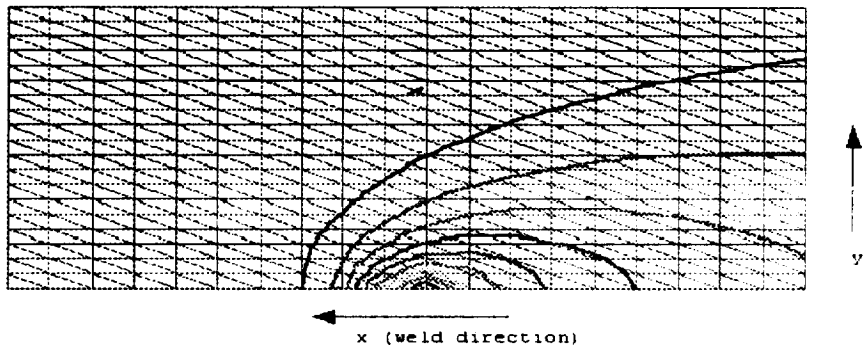

Figure 11. Computed Isotherms around Model of Friction Stir Weld

In this figure the tool is assumed to move to the left. The value for b was set as the weld plug radius. This choice does not reflect the actual heat transfer area (a semi-circle) but does not distort the width of the initial disturbance. The plot shown also has a triangular grid on which the contours are plotted. The grid was used only to plot the contours and was generated after the temperature field was calculated. The relatively good agreement between predicted temperatures and measured maximum temperature indicates a balance between measured power input and measured temperature but does not represent a real predictive capability.

Conclusions:

Approximate computations of Friction Stir Welding forces and temperatures can be made based upon either a Mixed Zone or a Single Slip Surface model. The slip system operated with minimal force will be initiated before any other slip system can operate and hence in general computed loads and powers should be regarded as upper bounds

Although physically neither model has yet been excluded, computational inconsistencies with the Mixed Zone model favor the Single Slip Surface model.

Slip surface profiles computed for the Single Slip Surface model resemble the boundaries of observed in FSW cross sections. Observed cross sections also exhibit what seems to be slower, secondary rotational flows with axes parallel to the weld travel direction; these are thought to be a result of the downwards flow induced by screw threads on the pin tool. Asymmetry of the forward-moving and backward-moving edges of the tool shoulder is also reflected in observed cross-sectional asymmetries.

Acknowledgements:

This paper is the result of the efforts of many people. The work was performed at the Marshall Space Flight Center through NASA's Summer Faculty Fellowship program (Grant NGT-52819), which supported the three faculty member authors, in cooperation with FSW research and development specialists Jeff Ding (NASA) and Peter Oelgoetz (Boeing). Dr. Biliyar Bhat, Chief of the Metallurgical Research and Development Branch, was very generous in his support in equipment and analytical services.

References:

1) Nunes, A.C., Jr., (1997) "Friction Stir Welding Process Analysis: A Progress Report". Proceedings of Friction Stir Welding Workshop, Marshall Space Flight Center, February 24, 1997. (To be published).
2) Miller, A.K., (1987), Unified Constitutive Equations for Creep and Plasticity, Elsevier Applied Science, London
3) Besseling, J.F., and van der Giessen, E., (1994), Mathematical Modeling of Inelastic Deformation, Chapman and Hall, London.
4) Gilman, J.J., (1969), Micromechanics of Flow in Solids, McGraw-Hill, Inc. New York.
5) Argon, A.S., (1975), Constitutive Equations in Plasticity, The MIT Press, Cambridge, MA.
6) Carslaw and Jaeger, (1957), Heat Conduction, Oxford University Press, Oxford.
7) Ambromowitz and Stegun, (1964), Handbook of Mathematical Functions, National Bureau of Standards, U.S. Department of Commerce.
8) McClure, J.C. University of Texas at El Paso. Private Communication. 1997.
9) ASM Metals Handbook, 10th Edition, Vol. 2, Properties and Selection: Nonferrous Alloys and Special Purpose Materials. P.79.